Supporting Information

Rapid sequential *in situ* multiplexing with DNA-Exchange-Imaging in Neuronal Cells and Tissues

Yu Wang,[1,2,3,9] Johannes B. Woehrstein[1,2,15], Noah Donoghue,[1,3,13] Mingjie Dai,[1,2,10] Maier S. Avendaño,[1,2] Ron C.J. Schackmann,[4] Jason J. Zoeller, [4] Shan Shan H. Wang,[5,11] Paul W. Tillberg,[7,12] Demian Park[7], Sylvain W. Lapan[3], Edward S. Boyden,[6,7], Joan S. Brugge,[4] Pascal S. Kaeser,[5] George M. Church, [1,3] Sarit S. Agasti,[1,2,14,*], Ralf Jungmann,[1,2,15*] Peng Yin.[1,2,*]

1. Wyss Institute for Biologically Inspired Engineering, Harvard University, Boston, Massachusetts, 02115, USA.
2. Department of Systems Biology, Harvard Medical School, Boston, Massachusetts, 02115, USA.
3. Department of Genetics, Harvard Medical School, Boston, Massachusetts, 02115, USA.
4. Department of Cell Biology, Harvard Medical School, Boston, Massachusetts, 02115, USA.
5. Department of Neurobiology, Harvard Medical School, Boston, Massachusetts, 02115, USA.
6. Department of Biological Engineering, Massachusetts Institute of Technology (MIT), Cambridge, Massachusetts, 02139, USA.
7. Media Lab, MIT, Cambridge, Massachusetts, 02139, USA.
8. Department of Brain and Cognitive Sciences, MIT, Cambridge, Massachusetts, 02139, USA.
9. Program in Biological and Biomedical Sciences, Harvard Medical School, Boston, Massachusetts, 02115, USA.
10. Program in Biophysics, Harvard University, Boston, Massachusetts, 02138, USA.
11. Program in Neuroscience, Harvard Medical School, Boston, Massachusetts, 02115, USA.
12. Department of Electrical Engineering and Computer Science, MIT, Cambridge, Massachusetts 02139, USA.
13. Warren Alpert Medical School, Brown University, Providence, Rhode Island, 02903, USA.
14. Present address: New Chemistry Unit and Chemistry & Physics of Materials Unit, Jawaharlal Nehru Centre for Advanced Scientific Research (JNCASR), Bangalore, India.
15. Present address: Department of Physics and Center for Nanoscience, Ludwig Maximilian University, 80539 Munich, Germany, Max Planck Institute of Biochemistry, 82152 Martinsried near Munich, Germany.
*Emails: P.Y. (py@hms.harvard.edu; 617-432-7731), R.J. (jungmann@biochem.mpg.de), and S.S.A. (sagasti@jncasr.ac.in)

Methods

Cultured cells preparation and staining

All animal procedures were in accordance with the National Institute for Laboratory Animal Research Guide for the Care and Use of Laboratory Animals and approved by the Harvard Medical School Committee on Animal Care and the Massachusetts Institute of Technology Committee on Animal Care.

Hippocampal neuron cultures were prepared from postnatal day 0 or 1 mice and plated on eight-well Lab-Tek II chambers with a density of 10,000 ~ 15,000 cells per well. Cells were grown for 14 days before fixation. Neurons used in Figure 2 were fixed using precooled methanol at -80 °C followed by three 5 minute PBS washes. Neurons used in other figures were fixed using 4% formaldehyde for 15 minutes at 37 °C, followed by quenching in 50 mM NH_4Cl for 10 minutes. HeLa cell and BSC1 cells were plated on eight-well Lab-Tek II chambers (15,000 cells per well) and grown for 24 hours. BSC1 cells used in SIM experiments were fixed using 3% Paraformaldehyde (PFA), 0.1% Glutaraldehyde, and 0.1% Triton X-100 for 12 minutes. Cells used in other experiments were fixed with 4% PFA.

Cells were then permeabilized and blocked in 0.1% Triton X-100, 0.1% Tween20, 3% Acetyl-BSA and 5% normal donkey serum for 2 hours. Specimens were incubated with primary antibodies diluted in incubation buffer (0.1% Triton X-100, 0.1% Tween20, 3% IgG-free BSA) overnight at 4 °C, and then washed with washing buffer (0.1% Tween20, 1% IgG-free BSA) for five times (brief wash for the first two washes and 10 minute incubation for the other three washes). DNA-labeled secondary antibodies (Jackson ImmunoResearch, conjugated in house) diluted in incubation buffer were incubated with samples for 2 hours at room temperature and then washed as for primary antibodies. In multiplexed detection experiment in which primary antibody-DNA docking strand conjugates were used, the sample was left on the microscope to maintain the position for imaging. Conjugated primary antibodies were diluted in incubation buffer and incubated with samples for 2 hours at room temperature, followed by PBS wash as described above. Post-staining fixation using 4% paraformaldehyde for 10 minutes followed by 5 minute quenching is recommended but optional.

Brain tissue preparation and staining

Transgenic mice expressing cytosolic YFP under the Thy1 promoter (Thy1-YFP-H C57BL/6 strain) were anesthetized with isoflurane and perfused transcardially with ice cold 4% paraformaldehyde. Dissected brains were kept in 4% paraformaldehyde at 4 °C for 24 hours, and then sunk in 30% sucrose with 100 mM glycine for 24 hours. Brains were sliced into 6 μm slices on a cryotome (Leica CM1850UV). Slices were kept in PBS at 4 °C until mounted on No 1.5 coverslips. Brain slices were permeabilized and blocked with 0.1% Triton X-100, 0.1% Tween20, 3% Acetyl-BSA, 5% normal donkey serum and a mixture of polydT DNA (20, 25, 30, 40 mers with 1 μM for each) overnight at 4 °C. Primary antibodies were diluted in incubation buffer as for neuron culture and incubated with brain slices for 48 hours at 4 °C. Slices were then washed using washing buffer three times for thirty minutes each. Slices were then incubated with secondary antibodies that were diluted in incubation buffer for overnight at 4 °C, followed by washing as for primary antibodies.

Mouse retina section preparation and staining

Animals were given a lethal dose of sodium pentobarbital (120 mg/kg) (MWI, 710101) and enucleated immediately. Eyes were removed and fixed in PFA for 15-30 min. Following dissection, retinas were immersed in 30% sucrose overnight prior to freezing in TFM (EMS, 72592) and cryosectioning at 40 μm. Coverslips were treated with poly-D-Lysine overnight, followed by PBS washes. Retina sections were washed with PBS + 0.3% Triton X-100 for three times with five minutes per wash. They were then blocked and stained as above. Note that SV2 was stained using DNA-primary antibody conjugates whereas other targets were stained using primary antibodies followed by DNA-secondary antibody conjugates.

Breast tumor section preparation and staining

Ductal carcinoma *in-situ* tumors were generated using the SUM225 cell line as described previously[1]. Tumor tissues were formalin fixed and paraffin embedded. 4 μm sections were mounted onto coverslips (24 × 50 mm no.1.5 VWR #48393.241) pre-treated with Silane solution (Leica Biosystems #3803120) to prevent tissue detachment during processing. Slides were baked for 1 hour at 60 °C, followed by deparaffinization in 100% xylene (Sigma 534056) for 5 minutes twice, and rehydrated by ethanol series (2 time for 2 minutes each 100% with EtOH, 1 time for 2 minutes with 70% EtOH, 1 time for 2 minutes with 50% EtOH, 1 time for 2 minutes with 25% EtOH, 1 time for 5 minutes with ddH_2O). The coverslips were incubated in antigen retrieval solution (IHCworld Cat# IW-1100) and placed in a steamer (Black & Decker HS1050) for 40 minutes (cold start). Slides were allowed to cool to room temperature for 20 minutes, followed by two washes of 5 minutes in ddH_2O. Blocking was performed using 5% goat serum (invitrogen #16210) in 1× Tris-buffered saline (TBS) for 30 minutes at room temperature. Tissue sections were incubated in TBS with

2.5% goat serum containing anti-HER2 and anti-SMA primary antibodies for 1 hour at room temperature. Slides were incubated with DNA-conjugated secondary antibodies for 1 hour at room temperature and stored in TBS until imaging.

Diffraction-limited image acquisition

The diffraction-limited images in Figure 2, Figure 3c and Figure S1-3, 6 and 10 were acquired with a Yokogawa spinning disk confocal CSU-X1 unit on a Nikon Ti inverted microscope. Figure 2 and Figure S1-3 and 10 were acquired using a 100× Plan Apo NA1.4 oil-immersion objective whereas Figure 3c and Figure S6 were acquired using a 20× / 0.75 NA dry objective with additional 1.5× magnification. Alexa488 was visualized using the 488 nm laser (1.74 mW, out of objective) and 525/50 emission filter; YFP was visualized using the 515 nm laser (1.89 mW) and 535/30 emission filter; Cy3b was visualized using 561 nm laser (4.02 mW) and 620/60 emission filter; Atto655 was visualized by the 647 nm laser (7.2 mW) and 700/75 emission filter. Images were collected with an ORCA-AG cooled CCD camera from Hamamatsu and Metamorph software. Camera exposure time was kept at 5 seconds for Figure 2 and 0.75 second for Figure 3. Z-stacks were collected with a z-step size of 140 nm for Figure 2.

In Figure 2, SynapsinI, vGAT, MAP2, pNFH and AlphaTubulin were stained using primary antibodies from five species, followed by DNA-conjugated secondary antibodies. After imaging, two primary antibodies that are directly conjugated with DNA docking strands were introduced to target AcetylTubulin and GFAP, surpassing the limitation of available antibody species. Sequential imager strand application was performed manually with gel-loading tips. Imager strands were diluted in 1× PBS/ 500 mM NaCl with a concentration of 10 nM. 1× PBS with 0.1% Tween 20 was used as washing buffer to remove imager strands.

The images in Figure 3a and b and Figure S4, 11 were acquired using a Zeiss Axio Observer with LSM 710 scanning confocal system. The images were 1024*1024 pixels and acquired at acquisition speed 7. Each image was acquired by averaging 4 images. The retina multiplexing experiment was performed by six rounds of buffer exchange of Cy3b-tagged imager strands. The laser intensity and exposure time were kept the same for the negative control group and experiment group in Figure S4. The scale was adjusted to the same range using FIJI for comparison. To facilitate imager strand removal in thick tissue sample, 0.1× PBS with 0.1% Tween 20 was used as washing buffer in the exchange tissue imaging experiment.

Multiplexed Structured Illumination image acquisition

BSC1 cells grown in Lab-Tek chambers were fixed and stained with primary antibodies targeting alphaTubulin, betaTubulin, Tom20 and Vimentin, followed by DNA-conjugated secondary antibodies. Alexa488-conjugated anti-chicken (Vimentin) secondary antibodies was added along with DNA-conjugated secondary antibodies in about 1:10 ratio (dye conjugated and DNA-conjugated anti-chicken antibodies). Antibodies were fixed using 4% PFA after staining. The multiplexed images were acquired by four rounds of buffer exchange of Cy3b-tagged imager strands. All 3D-SIM data was collected on a Zeiss ELYRA system with a 63×/1.40 N.A Plan Apo oil immersion objective lens. Image stacks were acquired with a z-step of 150 nm and with 25 raw images per plane (five phases and five angles). Super-resolution images were computationally reconstructed from the raw data set with a built-in algorithm in the Zeiss software. Buffer exchange was performed using flow cell chambers described in Jungmann and Avendaño et al.[2]. Glox oxygen scavenger system was added to the imaging buffer to prevent photobleaching. 0.1× PBS was used as washing buffer to facilitate imager strand removal.

Multiplexed STED image acquisition

Images were acquired using Leica SP8 X with STED 3X microscope system. Leica 100X/1.4 oil objective specialized for STED imaging is used. Green and Red channel laser/detection were set up as 488 nm/(500-540 nm) and 561 nm/(570-630 nm). Imaging was performed at zoom 5 with 1024 × 1024 format, yielding 23 nm pixel size to match STED imaging resolution requirement. Multiple

line accumulation and frame average were used to increase STED image Signal-to-Noise quality. SynapsinI was stained also with Alexa488-conjugated secondary antibodies and its signal from 488 nm laser channels were used for image registration.

Super-resolution Exchange-PAINT image acquisition

Images were acquired using an inverted Nikon Eclipse Ti microscope, applying an objective-type TIRF configuration using a Nikon TIRF illuminator with a 100×, NA1.49 oil-immersion objective (CFI Apo TIRF). Two sets of lasers and emission filters were used: 488 nm (200 mW nominal, Coherent Sapphire) / ET525/50 nm and 647 nm (300 mW nominal, MBP Communications) / ET700/75 nm. Images were captured on an electron-multiplying (EM) CCD camera (iXon X3 DU-897, Andor Technologies). The CCD readout rate was set to 3 MHz at 16 bit and 5.1 pre-amp gain. No EM gain was used. 30,000 frames with 100 ms integration time were acquired for each target. 80 nm gold nanospheres (Microspheres-Nanospheres) were used as fiducial markers for drift and alignment markers. The z-axis focal planes were kept constant for all the synaptic proteins, SynapsinI, Bassoon, vGAT and Gephyrin, while the focal planes were adjusted for four other structural proteins to obtain images of optimal quality. Sequential imager strand application was performed manually with gel-loading tips. Imager strands were diluted in 1× PBS/ 500 mM NaCl with a concentration of 3 nM. 1× PBS with 0.1% Tween 20 was used as washing buffer to remove imager strands.

Image processing and analysis

For super-resolution PAINT images, the time-lapse imaging movies were saved as Raw Data using FIJI and imported into custom-written program in MATLAB. The final images were reconstructed using spot-finding and 2D-Gaussian fitting algorithms. A simplified version of this software is available for download at http://molecular.systems/software or http://www.dna-paint.net. The image alignment for the merged synaptic protein image was performed by overlaying gold nanoparticles manually.

Image registration for diffraction-limited data acquired by the spinning disk confocal microscope was performed as follows: since samples were maintained on the stage and all microscope settings were kept the same during the entire experiment, only rigid transformation (translation and rotation) will be considered and corrected. The spinning disk confocal microscope contained the Nikon perfect focus system to maintain z-position. Therefore, drifts in only x- and y-axis were corrected. Signals from 488 nm laser channel were captured in every exchange cycle and served as the reference for sample drift. Images were first corrected for translation using a Fast Fourier Transformation (FFT)-based phase correlation algorithm, and then corrected for rotation using a Harris feature extraction and matching algorithm with Matlab built-in functions. The transformation matrices were applied to target images.

Image registration for 3D diffraction-limited retina imaging was performed using an algorithm developed by Hunter Elliott from Harvard Medical School Image and Data analysis core. The images were first filtered with a gradient filter and the intensity was then normalized. 3D FFT- based phase correlation was performed to calculate the image shift.

Subpixel Image registration for SIM and STED was performed based on an algorithm developed by Guizar-Siciros M, et al.[3] (the Matlab code is available from Mathworks and the detailed algorithm was described in the original paper). The initial code was written for 2D image registration but it can be extended to 3D by adding one dimension. For 3D SIM data, the reference image f and target image g were first converted to frequency domain F and G using FFT. The normalized cross-spectrum is defined as $R = F \times G^* / |F \times G^*|$, where G^* denotes the complex conjugate of G. To have an upsampling factor of 2, R was zero padded into a larger array of dimension (2x, 2y, 2z). This number can be further increased. However, it can be very computationally expensive. Further upsampling was achieved in the 1.5x1.5 pixel region of the estimated peak of cross-correlation using matrix multiplication discrete Fourier Transformation. For STED data, only 2D image registration was performed using the same method.

Cross correlation studies for Figure 2 and Figure S3 were performed using normxcorr2 function in Matlab.

Antibody-DNA conjugation

The conjugation involves crosslinking of thiol-modified DNA oligonucleotidess to Lysine residues on antibodies[4]. In brief, 250 uM 5' thiol-modified DNA oligonucleotides (Integrated DNA Technologies) were activated by 100 mM DTT for 2 hours and then purified using NAP5 columns (GE Healthcare Life Sciences, 17-0853-02) to remove excessive DTT. Antibodies formulated in PBS only were concentrated using 100KDa Ambicon Ultra Filters (EMDMillipore, UFC510096) to 2 mg/ml and reacted with maleimide-PEG2-succinimidyl ester crosslinkers (Singma 746223) for 2 hours. Antibodies were then purified using 0.5ml 7kDA Zeba desalting columns (LifeTechnologies, 89883) to remove excessive crosslinkers. Activated DNA oligonucleotides were incubated with antibodies (11:1 DNA: Antibody ratio) overnight at 4 °C. Final conjugated antibodies were washed using PBS/BSA (100ug/ml) in Ambicon Ultra Filters four times to remove nonreacted DNA oligonucleotides. Conjugated antibodies were kept at 4 °C.

The SV2 antibody used in Figure 3 was conjugated using the SiteClick kit from ThermoFisher (S10467). The DBCO-modified DNA oligos were purchased from Boston Open Labs.

Supplementary Figures and Tables

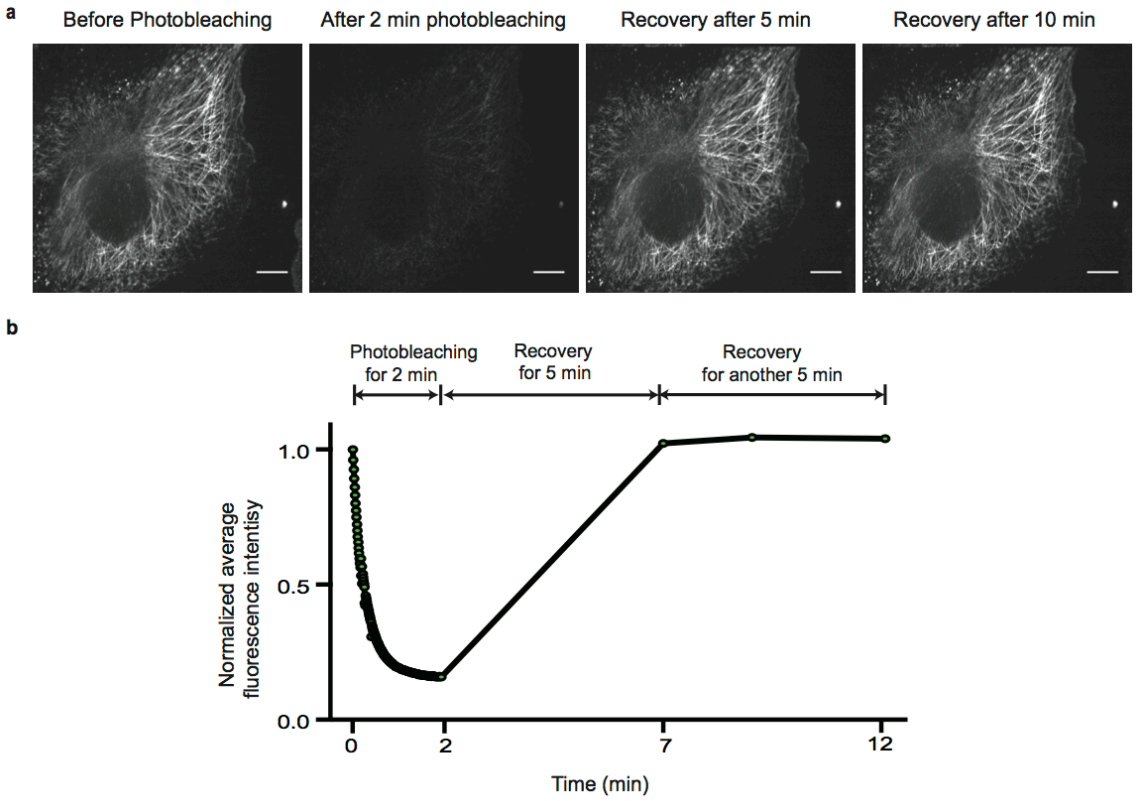

Figure S1. Fluorescent signal recovery after photobleaching in DNA-Exchange-Imaging. (**a**) BSC1 cells were stained for Beta-tubulin and imaged using Cy3b-conjugated imager strands. Photobleaching was performed using a 561 nm laser with 30 mW excitation power. Fluorescence signal decreased after photobleaching. A series of 200 images were taken in 2 min with 600 ms camera exposure time for each image. Fluorescence was then allowed to recover for 10 min. (**b**) Quantification of average fluorescence intensity of the images. The average fluorescence intensity dropped to 16% after 2 min of photobleaching and returned to ~100% after 5 minutes and remained the same afterwards.

Note: Fluophores can be typically photobleached upon sufficient long exposure to excitation lasers, and the rate of photobleaching depends on fluorophore species, the intensity of illuminating lasers and the buffer environment. Initial focusing and scanning of the specimen to locate the regions of interest often results in photobleaching of the fluorophores and hence undesired loss of fluorescent signals. Using conventional imaging methods with dye-conjugated antibodies, photobleaching is not reversible and leads to permanent loss of fluorescence signals. However, in DNA-Exchange-Imaging, due to the semi-transient nature of the binding interaction between the imager strand and docking strand, a photobleached imager strand will be eventually replenished by an unbleached one in the solution, allowing the full recovery of transiently bleached fluorescence signals at the target site. Scale bars: 10 µm.

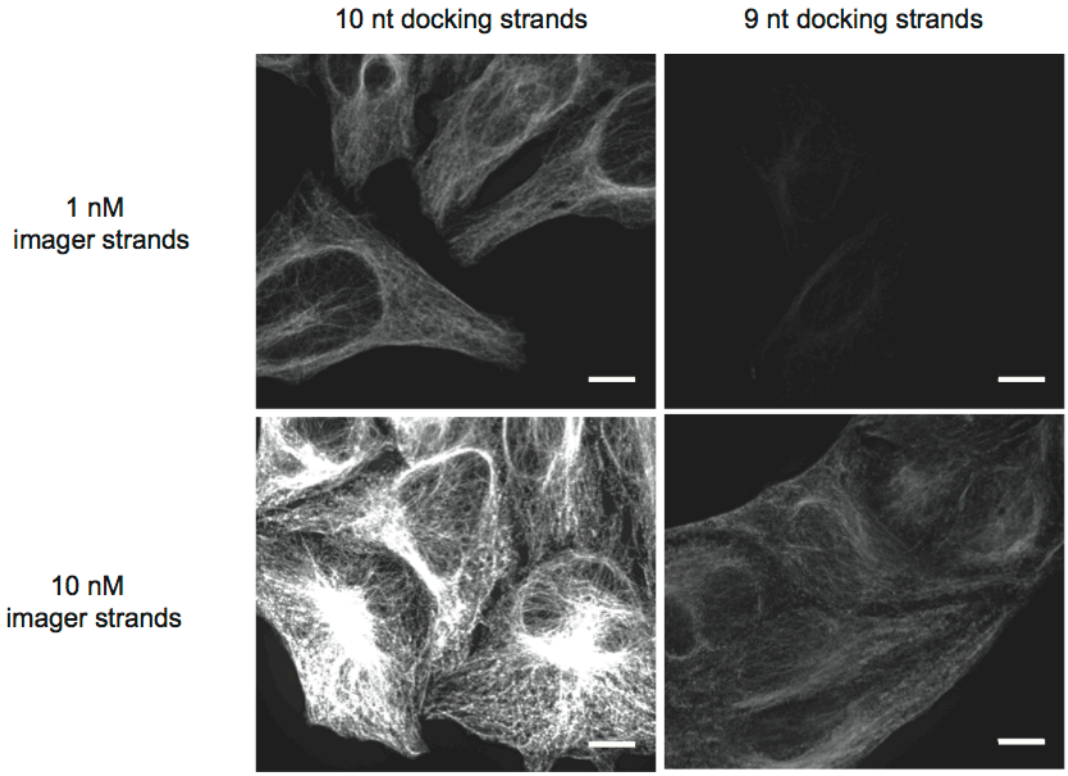

Figure S2. Comparison of image quality between 9 nucleotides (9 nt) DNA docking strands and 10 nucleotides (10 nt) DNA docking strands at different imager strand concentrations. Microtubules in HeLa cells were targeted using a rat alphaTubulin primary antibody. A donkey anti-rat secondary antibody, tagged with 9 nt docking sequence (Ab-TTGATCTACAT) or 10 nt (Ab-TTGATCTACATA) docking sequence, was used for indirect immunostaining. The sequence for imager strand is TATGTAGATC-dye. In diffraction-limited imaging, 10 nt docking strands perform significantly better than 9 nt. All images were taken using the same laser intensity and camera exposure time, and presented in the same scale for brightness. Scale bars: 10 μm.

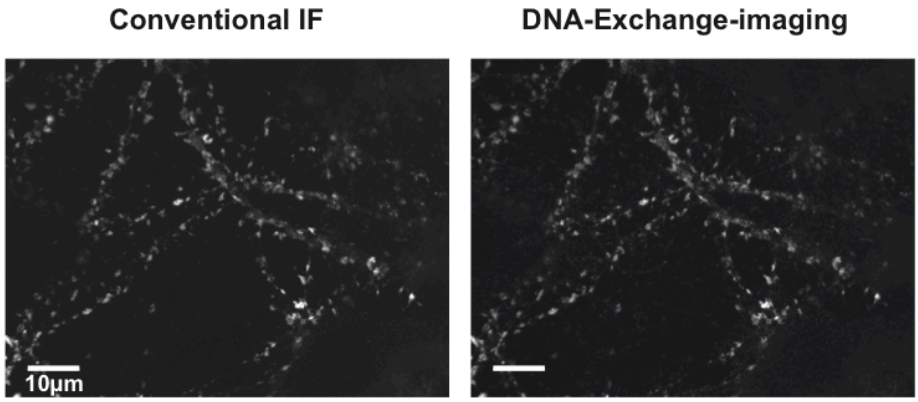

Figure S3. Comparison of SynapsinI signal imaged using conventional IF imaging and DNA-Exchange-imaging. Fixed DIV14 mouse hippocampal neurons were stained with SynapsinI primary antibodies, followed by both Alexa488-conjugated and DNA docking strands conjugated secondary antibodies (Ab-TTATGAATCTAC) as in the schematic. Images on the left were from conventional IF imaging taken with the 488nm laser channel. Images on the right were from DNA-Exchange-imaging taken with Cy3b-tagged imager strands under the 561 nm laser channel. Scale bars: 10 μm. Correlation Coefficient: 0.9607.

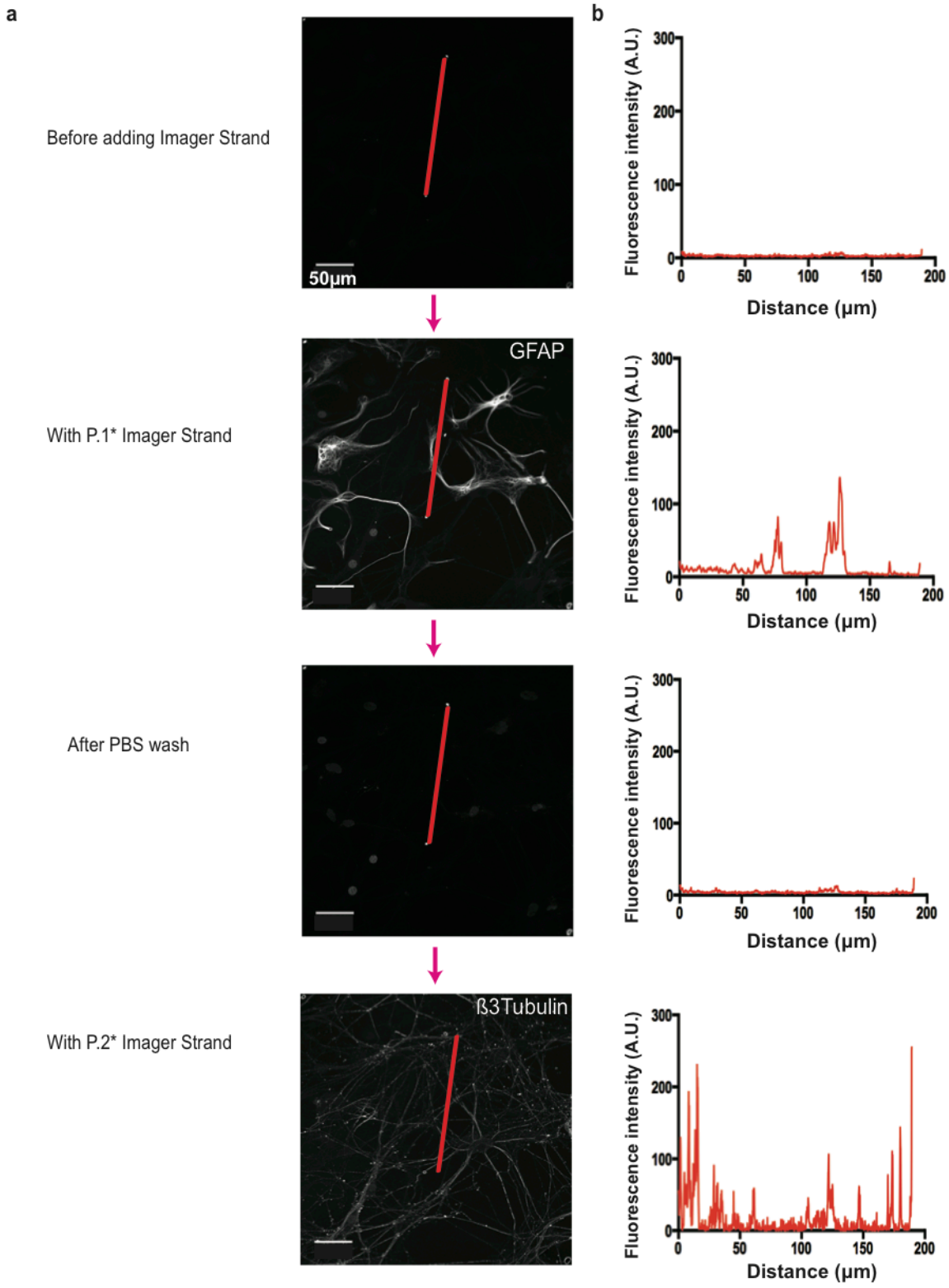

Figure S4. Efficiency of imager strand removal between imaging cycles based on fluorescence intensity measurement. Fixed DIV14 mouse hippocampal neurons were stained with antibodies targeting GFAP and beta3Tubulin. **(a)** P.1* imager strands (TATGTAGATC-Cy3b) were firstly introduced to specifically visualize GFAP followed by PBS wash for 5 minutes. P.2* imager strands (GTAATGAAGA-Cy3b) were then introduced to visualize beta3Tubulin. All images were adjusted to the same brightness scale. Scale bars: 50 μm. **(b)** Fluorescence intensity along the red line shown in (a).

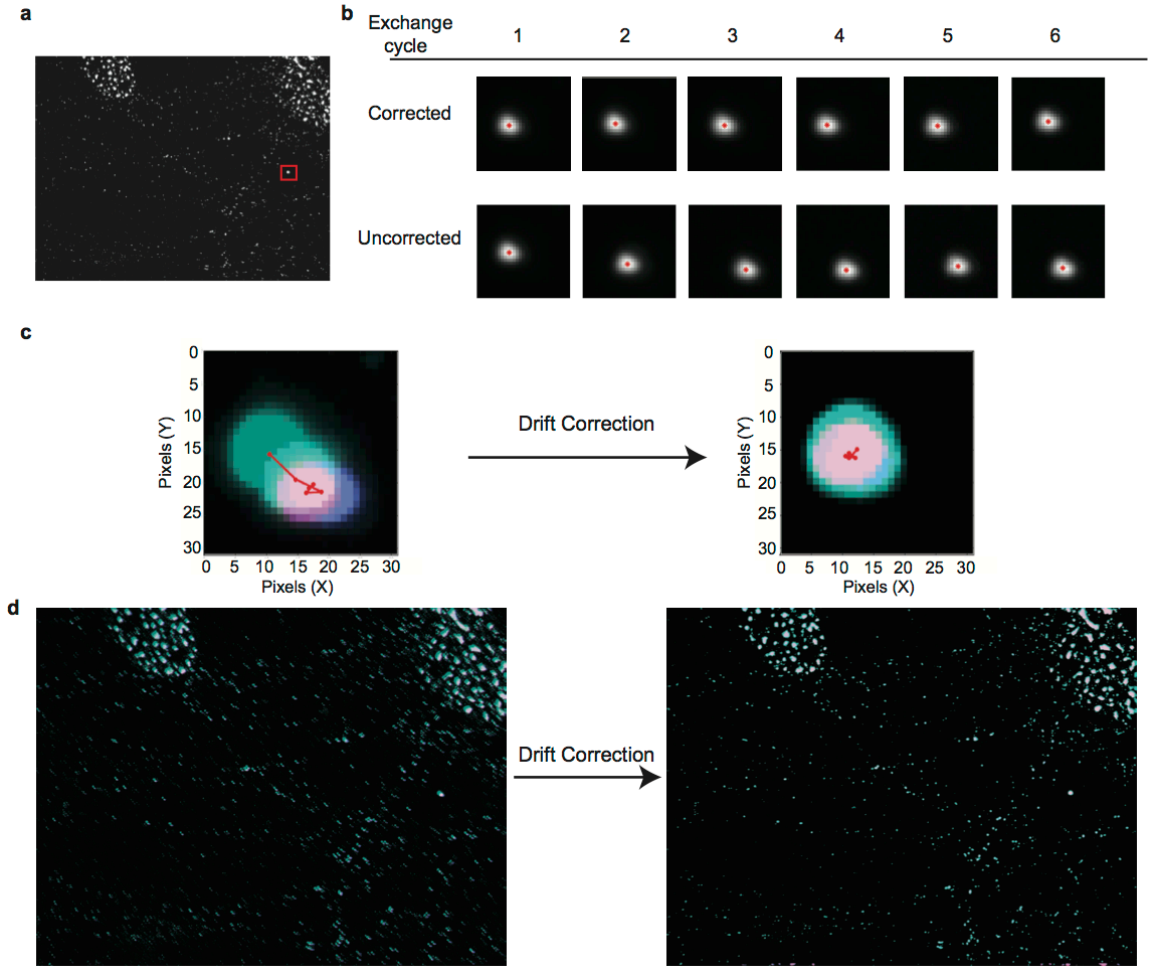

Figure S5. Drift correction of multiplexed diffraction-limited DNA-Exchange-imaging results from Figure2. (a) Images on 488 nm laser channel (stained using gephyrin primary antibodies followed by Alexa488-labeled secondary antibodies in this experiment) were imaged on every cycle of imaging along with other targets. The bright signal indicated in the red box region was used for demonstration in (b) and (c). **(b)** Comparison of the centroid positions of the selected marker in drift-corrected and uncorrected images from six cycles of imager strand exchange. The centroids were marked as red asterisks. **(c)** Track of centroid positions of the selected marker in merged images from (b). The x- and y- axis indicted the pixel value, and the whole image is 31 × 31 pixels with a pixel size of ~ 64 × 64 nm^2. **(d)** Comparison of uncorrected and corrected images.

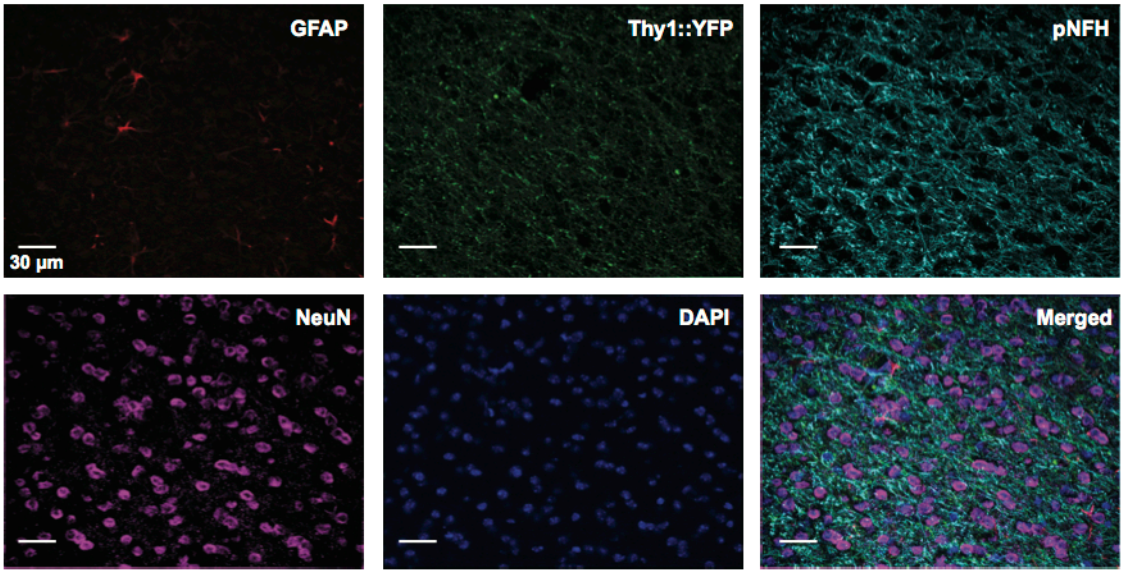

Figure S6. Five-target multiplexed diffraction limited imaging of mouse brain tissue sections. A 10 µm-thick mouse cortex section expressing Thy1::YFP was stained for GFAP, YFP, pNFH and NeuN. 2D images were taken using four rounds of exchange with Cy3b-tagged imager strands. The nucleus was stained with DAPI. Scale bars: 30 µm. DNA docking strand sequences are listed in **Table S6**.

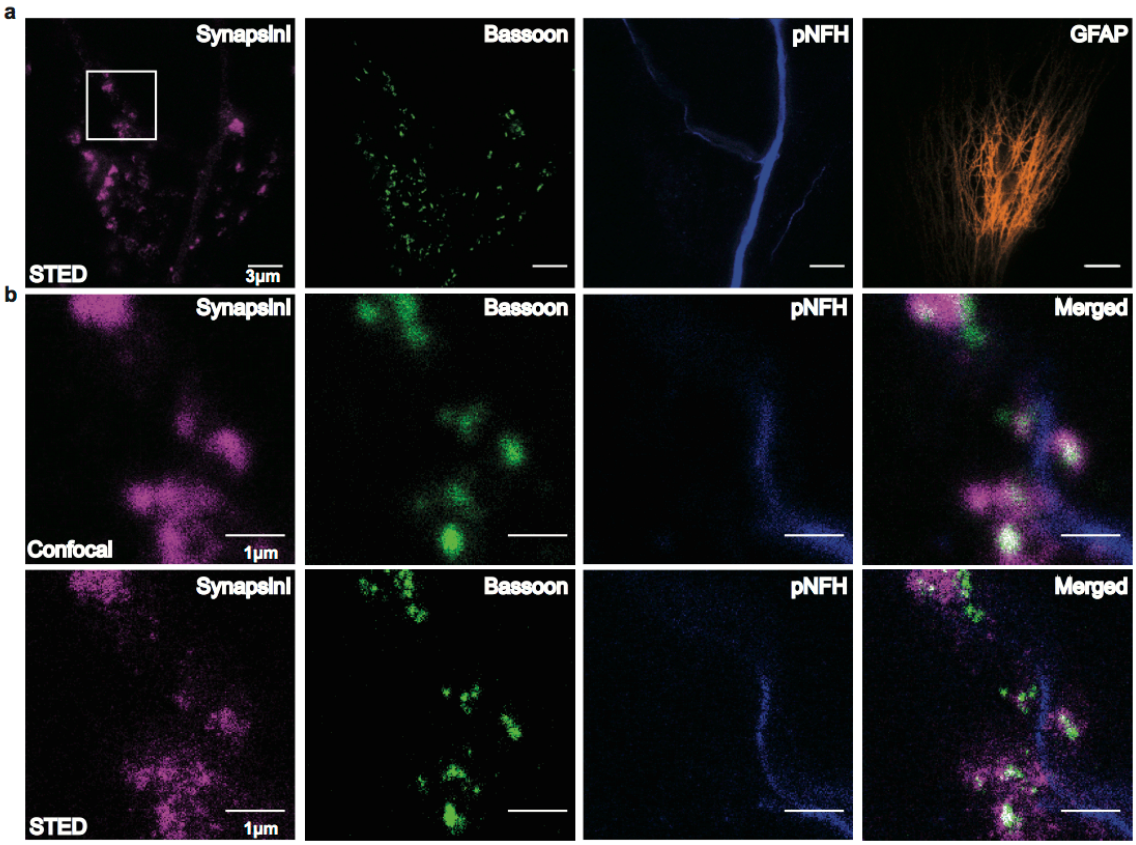

Figure S7. Multiplexed chromatic aberration-free Stimulated emission depletion (STED) imaging using DNA-Exchange-imaging. (a) Fixed DIV14 mouse hippocampal neurons were stained for GFAP, pNFH, SynapsinI and Bassoon. Four-round exchanges of Cy3b-conjugated imager strands were performed to acquire a 2D image for each target. It should be noted that GFAP was imaged in a region slightly under the other three targets because of the missing GFAP signal in the original region. Scale bar: 3 μm. **(b)** Magnified view of SynapsinI, Bassoon and pNFH from the white square region in (a). Confocal images of the same region are also presented for comparison. Scale bar 1 μm. DNA docking strand sequences are listed in **Table S9**.

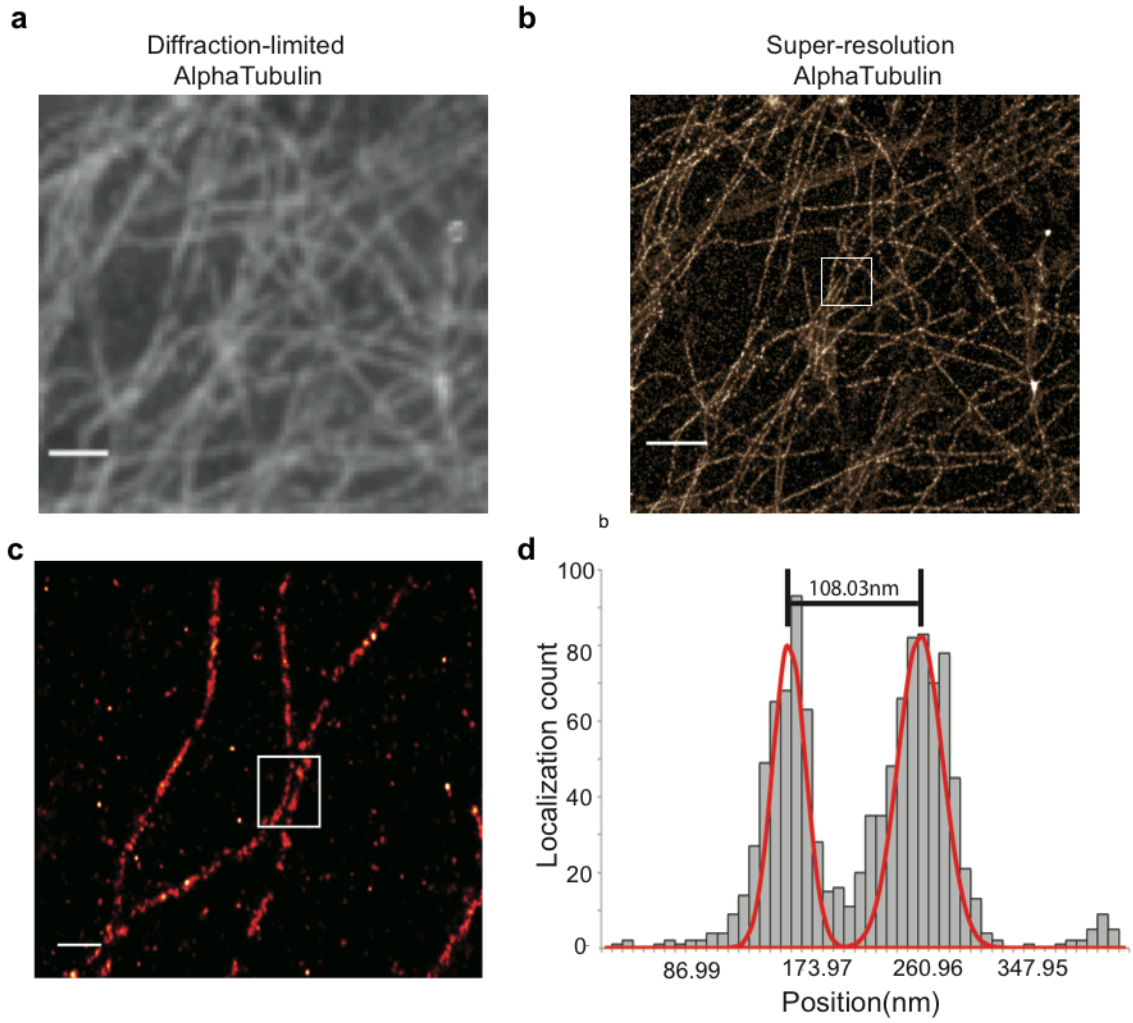

Figure S8. Super-resolved microtubule structure imaged with DNA-PAINT. (a) and **(b)** Comparison of diffraction-limited (a) and super-resolution (b) images of microtubules from Figure 5. Scale bar: 2 μm. **(c)** A magnified region from (b), where the region of analysis is indicated by a white box. Scale bar 500 nm. **(d)** Cross-sectional histogram of highlighted region in (c). The distance of the two microtubules is ~108 nm, well below the diffraction limit. The FWHM for the two microtubules are 44.8 nm and 68.0 nm, respectively.

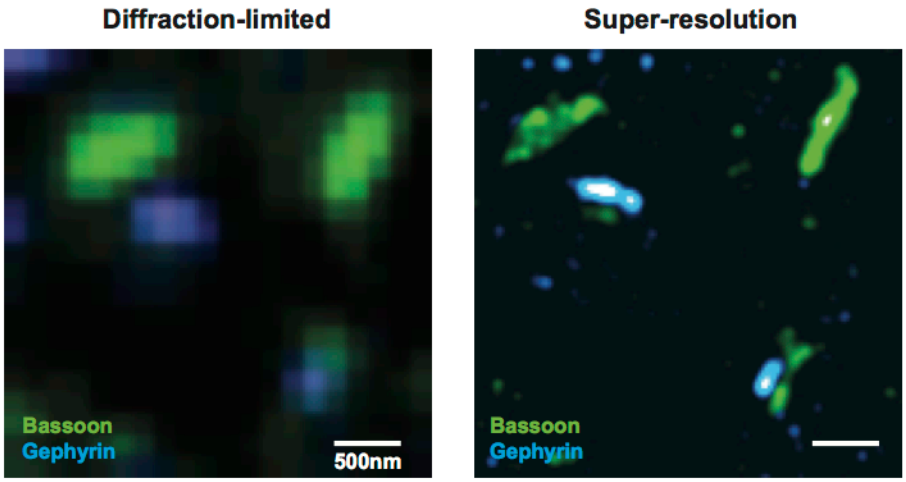

Figure S9. Visualization of presynaptic and postsynaptic proteins in diffraction-limited and super-resolved images. The left panel shows the view of Bassoon (presynaptic; Green) and Gephyrin (postsynaptic; Blue) in a diffraction-limited image. Bassoon and Gephyrin signals are not able to be separated. The right panel shows the view of Bassoon and Gephyrin in a super-resolved image where the signals are clearly distinguishable between the two. Scale bars: 500 nm.

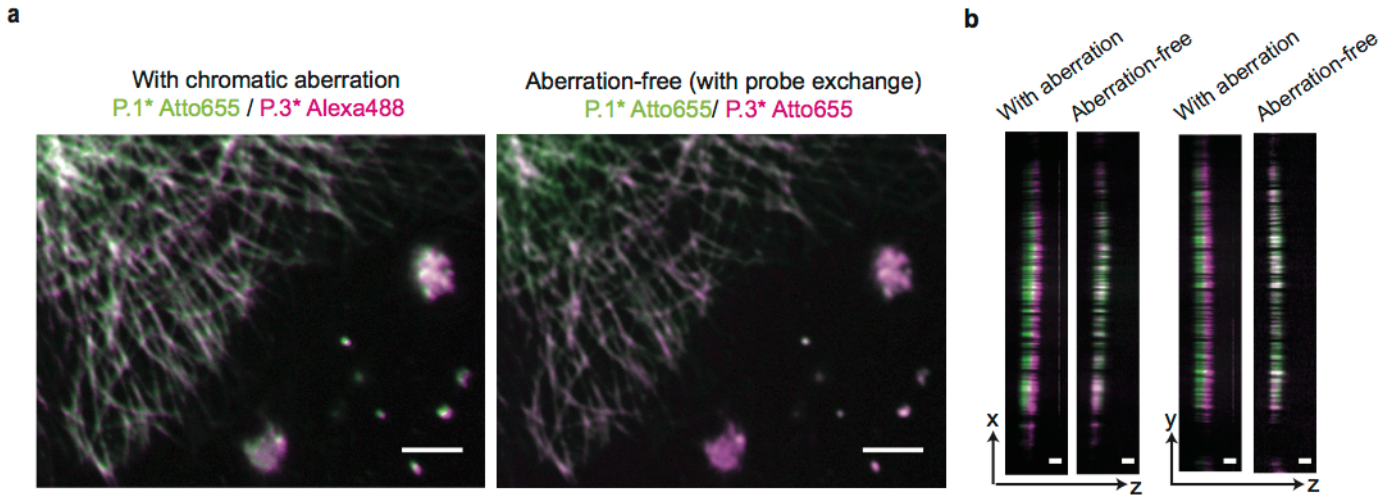

Figure S10. **Chromatic aberration-free imaging with DNA-Exchange-Imaging.** (**a**) Images with (left) and without (right) chromatic aberration. BSC1 cells were stained with primary antibodies against betaTubulin followed by two secondary antibodies, one with P.1 docking strands (Ab-TTATACATCTA) and the other one with P.3 docking strands (Ab-TTTCTTCATTA). The image with chromatic aberration was taken by addition of Atto655-conjugated P.1* imager strands and Alexa488-conjugated S.3* imager strands at the same time, whereas the image without chromatic aberration was taken by sequential addition of Atto655-conjugated P.1* and Atto655-conjugated P.3* imager strands. A z-stack of 101 images, each slice spaced 100 nm apart, covering ~10 µm z depth was acquired and subsequently projected onto a 2D plane for representation. An aberration-uncorrected 40× Plan Fluo lens was used in the experiment. In the image with chromatic aberration, although the target was the same, images for P.1 and P.3 docking sites that were taken using two laser channels (642 nm for Atto655 dye and 488 nm for Alexa488 dye) were shifted from each other. In contrast, DNA-Exchange-Imaging allows the two types of docking strands to be imaged using imager strands conjugated to the same species of dye (Atto655). As a result, the chromatic aberration was avoided and no shift was observed. It should be noted that any drift caused by buffer exchange in DNA-Exchange-Imaging was corrected using a reference image. In this experiment, the reference image was betaTubulin signal taken from 488 nm laser channel. That is, in the first round of imaging, Atto655-P.1* and Alexa488-P.3* were added and images were acquired for both channels; in the second round of imaging, Atto655-P.3* and Alexa488-P.3* were added and images were acquired for both channels. The drift was calculated using an algorithm to perform cross-correlation of the two reference images from the Alexa488 channel, and the images from the Atto655 channel were shifted based on the calculated drift from reference images. Scale bars 5 µm. (**b**) z axial chromatic aberration comparison between images with and without chromatic aberration. Scale bar: 2 µm (the scale bar is for Z direction only as the z pixel size is 100 nm, i.e. same with sampling spacing, and the XY pixel size is 107 nm).

Note: Chromatic aberration is caused by the failure of lens to focus light of different wavelengths to the same convergence point. Chromatic aberration can cause the same object to appear at different locations when imaged using lasers with different excitation wavelengths. DNA-Exchange-Imaging uses only one fluorophore species and hence only one excitation laser to visualize all targets, and thus naturally avoids chromatic aberration for multiplexed imaging. It should be noted that certain lenses, for example Apochromat, have been designed to correct aberration. Unfortunately, the aberration cannot be completely eliminated and may cause problems when dyes with significant spectral difference (for example, 405 nm and 647 nm) are used in the same experiment. The problem can be exacerbated if an aberration-corrected lens is not available. However, we also note that aberrations can – in principle – be "calibrated" and corrected using fluorescent beads imaged at different wavelength and subsequent nonlinear affinity matrices can

be used to "map" different wavelengths onto each other. Compared with these alternative methods for aberration correction, DNA-Exchange-Imaging is unique in that it is naturally aberration-free.

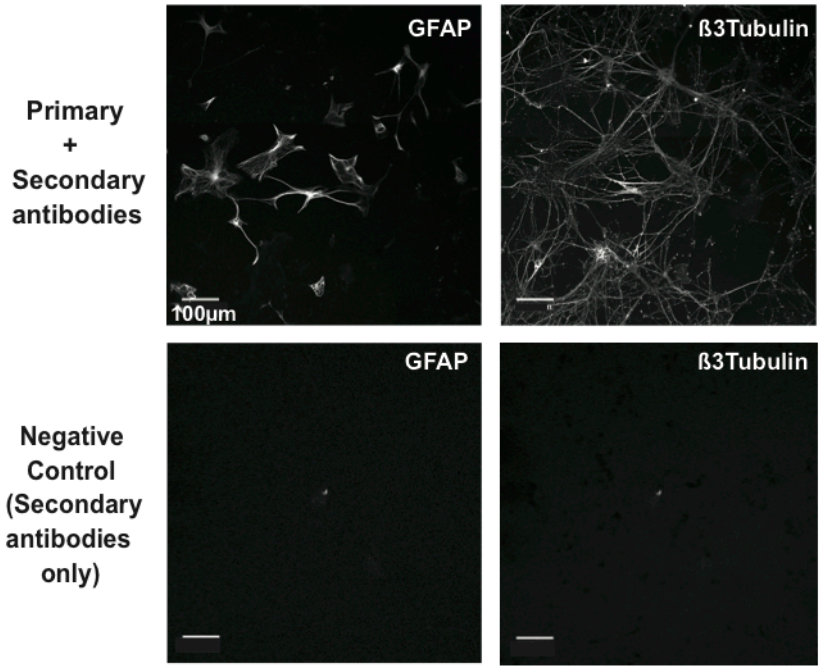

Figure S11. Test fluorescent signals caused by non-specific binding of DNA-conjugated secondary antibodies and fluorophore-conjugated imager strands. Fixed DIV14 mouse hippocampal neurons were stained with or without GFAP and beta3Tubulin primary antibodies, followed by DNA-conjugated secondary antibodies (Ab-TTATCTACATA for GFAP; Ab-TTTCTTCATTA for beta3Tubulin). The upper panel shows images taken from the sample stained with both primary and secondary antibodies, clearly distinguishing astrocytes and neurons. The lower panel shows images from the sample stained with secondary antibodies only, where no obvious signal can be observed. The laser intensities, camera exposure time and brightness scale were kept the same between two samples. Scale bar: 100 μm.

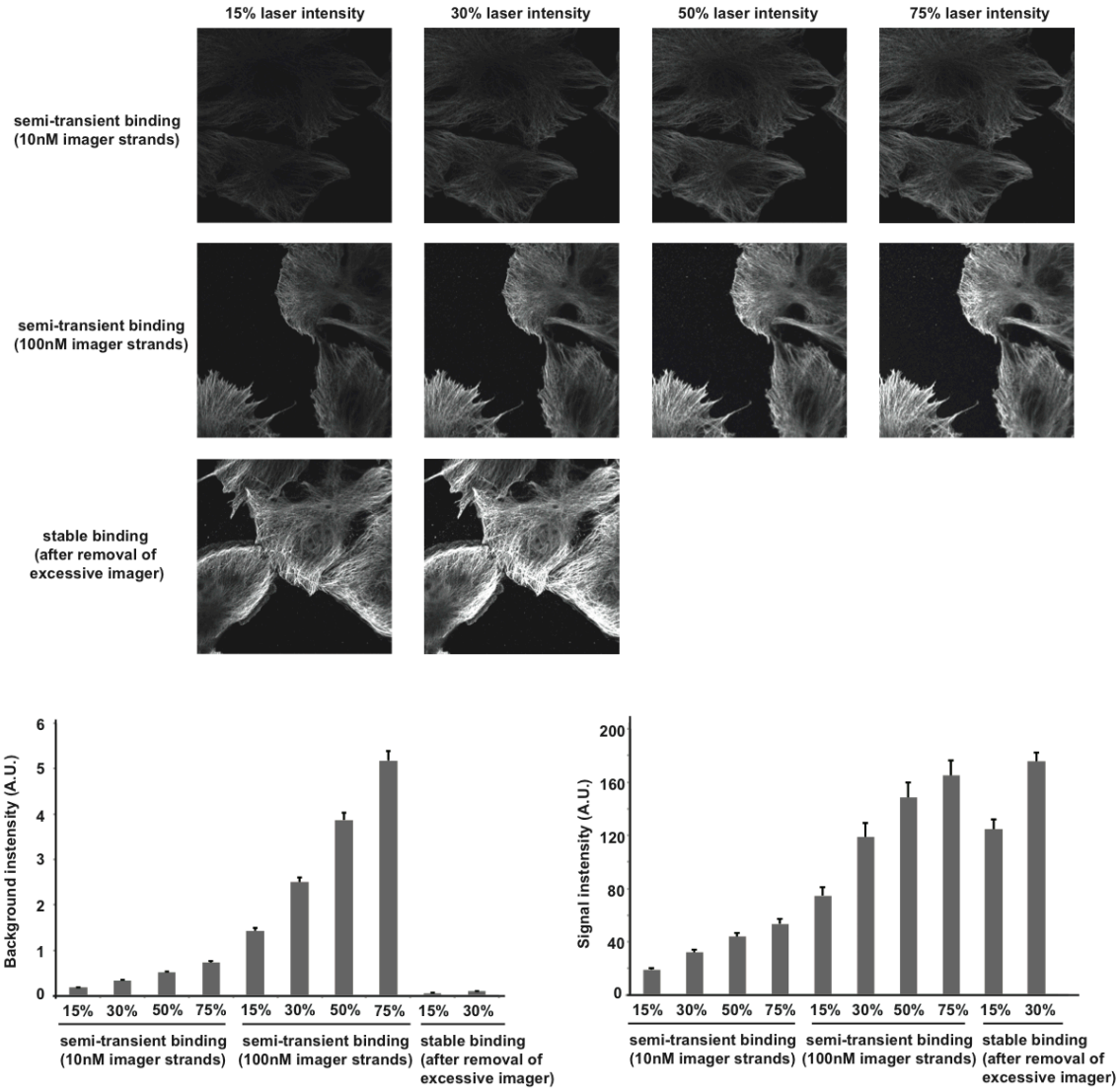

Figure S12. Comparison of imaging quality between semi-transient binding and stable binding schemes with microtubule targets. BSC1 cells were fixed and labeled with antibodies targeting Beta-Tubulin. Antibodies were conjugated with either 10-mer docking strands for semi-transient binding or 12-mer docking strands for stable binding (strand 1 used in Schueder et al.). For semi-transient binding, we added 10 nM or 100 nM Alexa647-imager strands for imaging. For stable-binding, we incubated the cells with 1μM Alexa647-imager strands for 1 hour followed by 3 times buffer washing with 5 minutes for each to remove excessive imager strands. The laser intensity was set to 15%, 30%, 50% or 75% with gain 600. All 8-bit images were displayed with the same scale of 0-255. The error bar is SEM, n = 6.

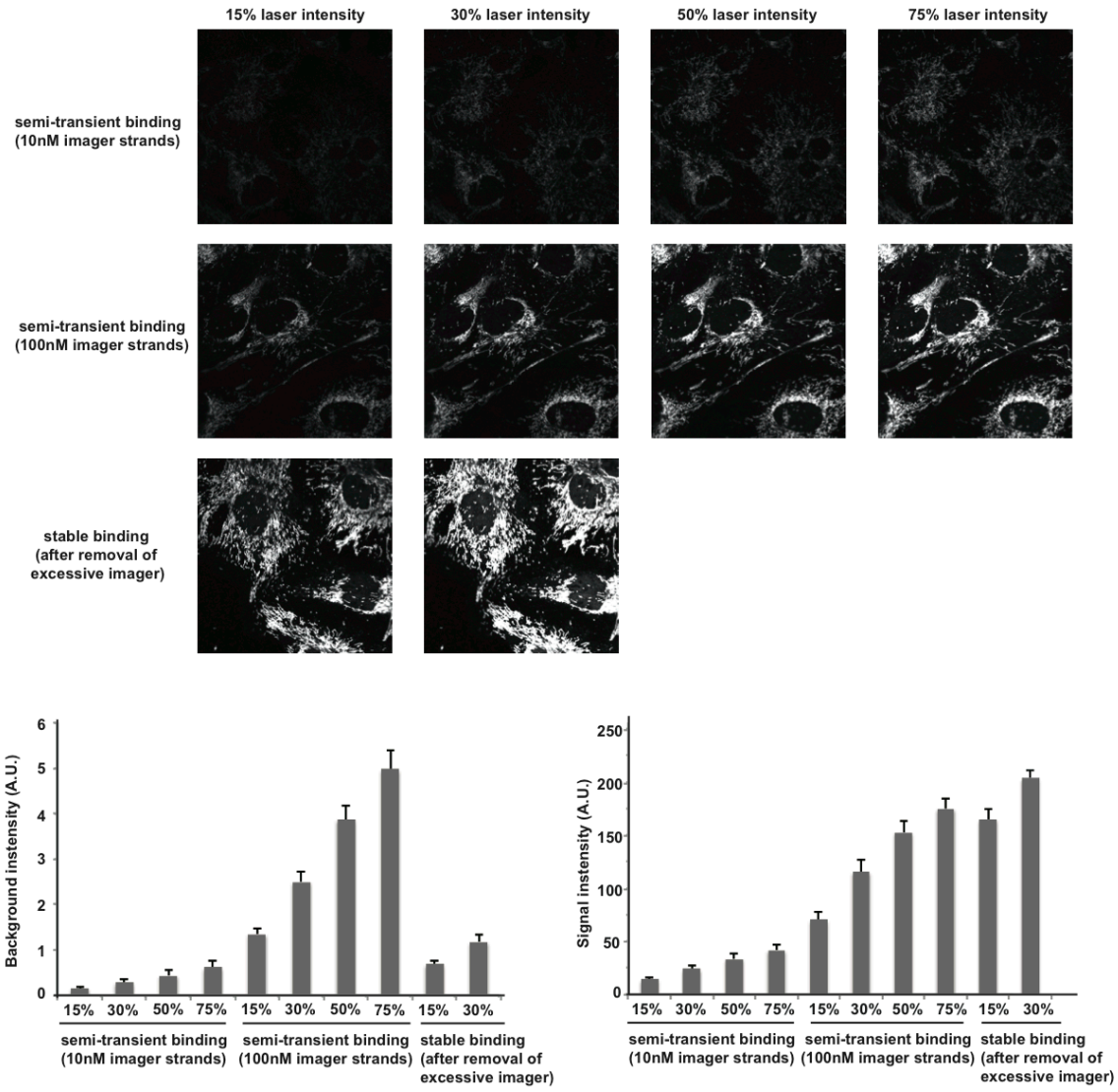

Figure S13. Comparison of imaging quality between semi-transient binding and stable binding schemes with mitochondria targets. BSC1 cells were fixed and labeled with antibodies targeting Tom20. Antibodies were conjugated with either 10-mer docking strands for semi-transient binding or 12-mer docking strands for stable binding. For semi-transient binding, we added 10 nM or 100 nM Alexa647-imager strands for imaging. For stable-binding, we incubated the cells with 1μM Alexa647-imager strands for 1 hour followed by 3 times buffer washing with 5 minutes for each to remove excessive imager strands. The laser intensity was set to 15%, 30%, 50% or 75% with gain 600. All 8-bit images were displayed with the same scale of 0-255. The error bar is SEM, n = 6.

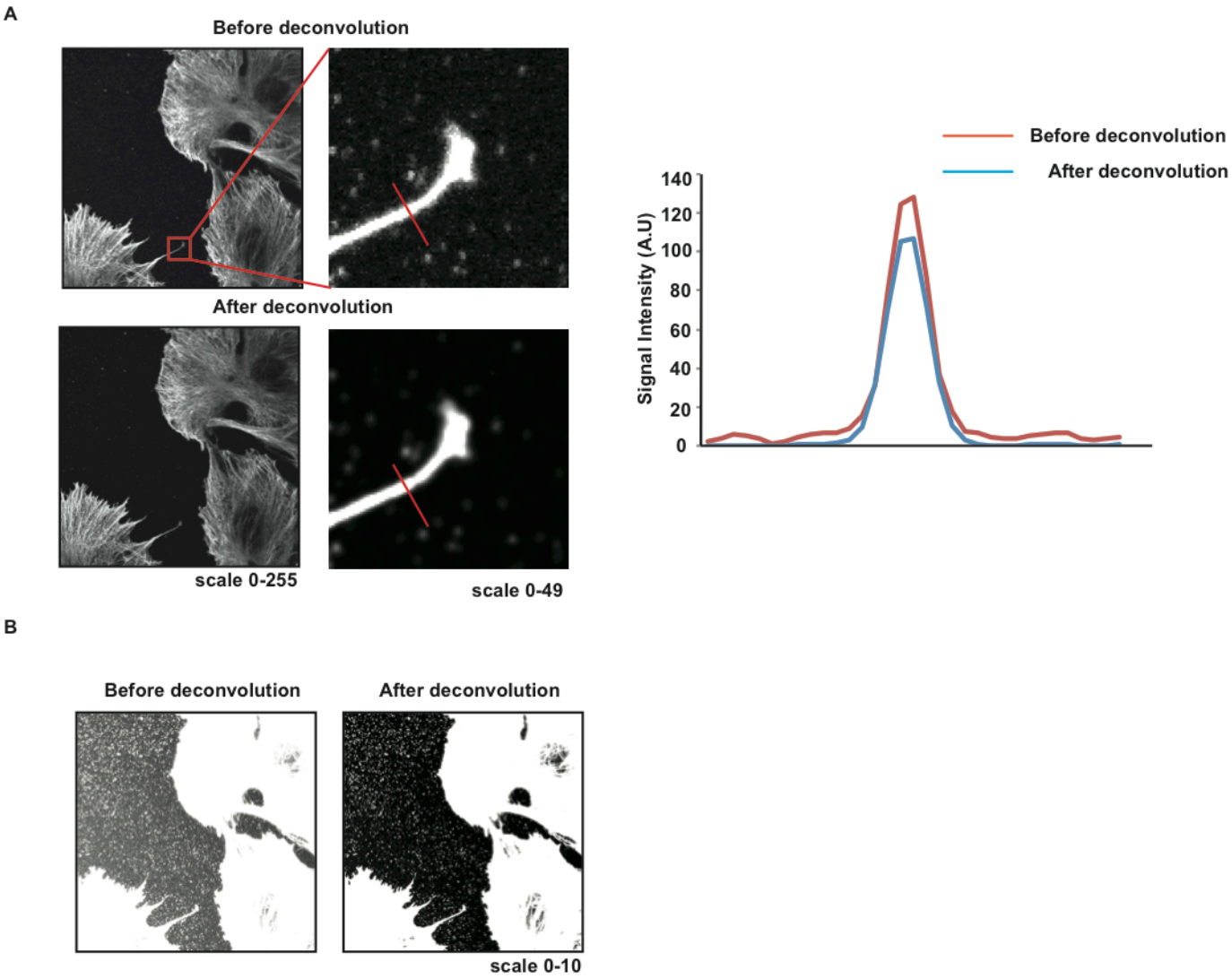

Figure S14. Image deconvolution on microtubule images in Figure S12. The deconvolution was performed using the Huygens software. A theoretical PSF and a deconvolution signal-to-noise parameter of 2 were used for deconvolution. **(A)** comparison of before and after deconvolution microtubule signals in semi-transient binding scheme (100nM imager strands at 75% laser intensity). One region in each image was selected for magnified view (marked in red square), and the signal profile of the indicated line was measured using FIJI. **(B)** The background of images was displayed by adjusting the contrast of the images.

Note: The results from Figures S12 and S13 were obtained under the same laser intensity illumination, stable binding scheme had higher signal, lower background and thus higher signal-to-background ratio compared with semi-transient binding. This is as expected because excessive imager strands in the buffer contribute to the background. In addition, in semi-transient binding scheme not all docking sites are occupied with imager strands, leading to decreased signals. Signal enhancement in semi-transient binding scheme can be achieved by further increasing the imager strands concentration (from 10 nM to 100 nM) to saturate the docking sites and by increasing laser intensity. Because of the continuous replenishment of imager strands in the semi-transient binding scheme, photobleaching is not a significant issue when laser intensity is high (also see **Figure S1**). Although semi-transient binding scheme had higher background, the background level was manageable and did not affect image visualization after adjusting the contrast. We think the low background attributed to the confocal imaging set up wherein the out-of-focus signal was blocked. This also applies to STED imaging. To further reduce background, we performed image deconvolution, an image processing method commonly used to improve image quality. It can be seen that after deconvolution, the signal of images became sharper and the background of image turned to ~0 in all images.

It should be noted that wide-field imaging could also be performed using semi-transient binding scheme if followed by image deconvolution. Indeed, the microscope used for the SIM experiment (**Figure 4**) is a wide-field microscope, and the SIM processing software automatically perform image deconvolution.

Comparison of DNA-Exchange-Imaging and other multiplexed protein imaging methods

Category	Subcategory	Method description	Reference	Comparison with DNA-Exchange-Imaging
Sequential antibody labeling	Antibody removal	Remove antibodies by denaturing using acidified glycine-SDS buffer or $KMnO_4$ or enzymatic digestion	5-8	1. The method requires repeated application of new antibodies after previous round of antibody removal or dye inactivation, and thus tends to be time consuming. Each round of staining typically takes 2 hours at room temperature and preferentially overnight at 4 °C for optimal labeling (e.g. Ref 9). 2. Harsh buffer treatment or laser treatment could potentially cause sample damage, e.g. cell loss. 3. Susceptible to photobleaching.
	Chemical bleaching of dyes	Dye inactivation using chemicals, e.g. 3% H_2O_2 and 20 mM NaOH	9, 10	
	Photobleaching of dyes	Dye inactivation with high power laser	11, 12	
Toehold mediated DNA probe replacement	-	Use eraser strand to remove dye-conjugated imager strand via toehold mediated branch migration	13, 14	1. The imager strand removal step requires explicit application of a complementary "eraser" strand that binds to the dye labeled imager strand. It thus involves more complex procedure and molecular constructs and tends to be more time consuming (e.g. in Ref.14, the imager removal took overnight compared with minutes in our DNA-Exchange-Imaging). 2. Susceptible to photobleaching as the imager strand is stably bound to the target before being explicitly removed using an eraser strand.
Spectral multiplexing	Quantum Dot	Use Q-Dots with more spectrally distinguishable colors than typical organic fluorophores	15	1. Limited multiplexing ability 2. Susceptible to chromatic aberration.
	Spectral imaging and linear unmixing	Integrate spectrum information with fluorescence imaging	16	1. Requires specialized instrument for spectrum detection 2. Uses computation algorithms to separate spectrally overlapping signals and is susceptible to artifacts generated by the unmixing algorithm.
	Spectrally resolved STORM	Integrate spectrum information with single-molecule based super-resolution STORM imaging	17	1. Uses single-molecule detection to separate spectrally overlapping signals, and is not directly applicable for diffraction-limited protein imaging. 2. Requires specialized instrument for spectrum detection.
Mass spectrometry imaging	Scanning mass cytometry (SMC) imaging	Laser ablation coupled with plasma time-of-flight mass spectrometry to detect isotope-labeled antibodies	18, 19	1. Destructive to samples. 2. Typically low resolution (1μm). 3. Require specialized instrument.
	Multiplexed ion beam imaging	Secondary ion mass spectrometry based ion beam scanning to detect isotope-labeled antibodies	19, 20	1. Repeated antibody staining (7 at a time) can be time-consuming. 2. Destructive to samples (although less than SMC). 3. Require specialized instrument.

Table S1. Overview of previous multiplexed protein target imaging methods and their comparison with DNA-Exchange-Imaging.

Description	Docking Strand Sequence	Imager Strand Sequence
P1	5’-TTTCTTCATTA-3’	5’-GTAATGAAGA-Dye
P2	5’-TTATCTACATA-3’	5’-TATGTAGATC-Dye
P3	5’-TTATGAATCTA-3’	5’-GTAGATTCAT-Dye
P4	5’-TTTCAATGTAT-3’	5’-CATACATTGA-Dye
P5	5’-TTAATTAGGAT-3’	5’-CATCCTAATT-Dye
P6	5’-TTAATTGAGTA-3’	5’-GTACTCAATT-Dye
P7	5’-TTTATATTGAC-3’	5’-CGTCAATATA-Dye
P8	5’-TTATGTTAATG-3’	5’-CCATTAACAT-Dye
P9 (10 nt)	5’-TTTCTTCATTAC-3’	5’-GTAATGAAGA-Dye
P10 (10 nt)	5’-TTGATCTACATA-3’	5’-TATGTAGATC-Dye
P11 (10 nt)	5’-TTATGAATCTAC-3’	5’-GTAGATTCAT-Dye
P12 (10 nt)	5’-TTAATTAGGATG-3’	5’-CATCCTAATT-Dye
P13 (10 nt)	5’-TTATGTTAATGG-3’	5’-CCATTAACAT-Dye
P14 (10 nt)	5’-TTAATTGAGTAC-3’	5’-GTACTCAATT-Dye
P15	5’-TTATAGTGATT-3’	5'-GAATCACTAT-Dye
P16 (10 nt)	5’-TTATACATCTAG-3’	5'-CTAGATGTAT-Dye
P17 (10 nt)	5’-TTTTAGGTAAAG-3’	5'-CTTTACCTAA-Dye
P18	5’-TTATAGTGATTC-3’	5'-GAATCACTAT -Dye

Table S2. DNA-Exchange-Imaging docking and imager strand sequences used in this study.

Target	Antibody	Species
AcetylTubulin	Invitrogen (32-2700)	Mouse
AlphaTubulin	ThermoFisher(MA1-80017)	Rat
Bassoon	Abcam (ab82958)	Mouse
Beta3Tubulin	ThermoFisher (MA1-19187)	Mouse
Chx10	ThermoFisher (PA1-12566)	Sheep
Cone arrestin	Millipore (AB15282)	Rabbit
Gephyrin	SynapticSystem (147108)	Human
GFAP	Invitrogen (13-0300)	Rat
GFAP	Encor (MCA-5C10-AP)	Mouse
GFP/YFP	Invitrogen (PA5-22688)	Rabbit
HER2	Dako #A0485	Rabbit
MAP2	SantaCruz (sc5359)	Goat
NeuN	Millipore (MAB377)	Mouse
pNFH	EnCor (CPCA-NF-H)	Chicken
SMA	Dako #M0851	Mouse
SV2	DSHB	Mouse
SynapsinI	Abcam (ab8)	Rabbit
SynapsinI/II	SynapticSystem (106004)	Guinea Pig
Synaptophysin	SynapticSystem (101004)	Guinea Pig
Tom20	SantaCruz (sc11415)	Rabbit
vGAT	SynapticSystem (131004)	Guinea Pig
Vimentin	Encor (CPCA-Vim)	Chicken
Vimentin	Biolegend (Poly29191)	Chicken

Table S3. Antibodies used in this study.

Target	DNA conjugates	Docking strand	Target	DNA Conjugates	Docking strand
SynapsinI	anti-rabbit secondary antibody	P11	GFAP	primary mouse antibody	P18
vGAT	anti-guinea pig secondary antibody	P12	MAP2	anti-goat secondary antibody	P13
pNFH	anti-chicken secondary antibody	P14	AlphaTubulin	anti-rat secondary antibody	P10
AcetylTubulin	primary mouse antibody	P15	Gephyrin	anti-human secondary antibody	Alexa488

Table S4. Antibodies and conjugated DNA docking strands for multiplexed diffraction-limited imaging in primary neuron culture.

Target	DNA conjugates	Docking strand	Target	DNA conjugates	Docking strand
SV2	primary mouse antibody	P16	GFAP	anti-rat secondary antibody	P10
Cone arrestin	anti-rabbit secondary antibody	P11	Chx10	anti-sheep secondary antibody	P13
Vimentin	anti-chicken secondary antibody	P14	Synapsin	anti-guinea pig secondary antibody	P12

Table S5. Antibodies and conjugated DNA docking strands for multiplexed diffraction-limited imaging in retina sections.

Target	DNA conjugates	Docking strand	Target	DNA conjugates	Docking strand
GFAP	anti-rat secondary antibody	P10	YFP	Anti-rabbit secondary antibody	P11
pNFH	anti-chicken secondary antibody	P14	NeuN	anti-mouse secondary antibody	P9

Table S6. Antibodies and conjugated DNA docking strands for multiplexed diffraction-limited imaging in mouse brain sections.

Target	DNA conjugates	Docking strand	Target	DNA conjugates	Docking strand
HER2	anti-rabbit secondary antibody	P11	SMA	anti-mouse secondary antibody	P9

Table S7. Antibodies and conjugated DNA docking strands for multiplexed diffraction-limited imaging in breast tumor sections.

Target	DNA conjugates	Docking strand	Target	DNA conjugates	Docking strand
alphaTubulin	anti-rat secondary antibody	P10	betaTubulin	anti-mouse secondary antibody	P9
Tom20	anti-rabbit secondary antibody	P11	Vimentin	anti-chicken secondary antibody	P17

Table S8. Antibodies and conjugated DNA docking strands for multiplexed SIM imaging.

Target	DNA conjugates	Docking strand	Target	Dna conjugates	Docking strand
SynapsinI	anti-rabbit secondary antibody	P11	Bassoon	anti-mouse secondary antibody	P9
pNFH	anti-chicken secondary antibody	P14	GFAP	anti-rat secondary antibody	P10

Table S9. Antibodies and conjugated DNA docking strands for multiplexed STED imaging.

Target	DNA conjugates	Docking strand	Target	DNA conjugates	Docking strand
SynapsinI	anti-rabbit secondary antibody	P3	Bassoon	anti-mouse secondary antibody	P1
vGAT	anti-guinea pig secondary antibody	P5	Vimentin	anti-chicken Secondary antibody	P6
Tom20	anti-rabbit secondary antibody	P4	AlphaTubulin	anti-rat secondary antibody	P2
GFAP	primary mouse antibody	P18	AcetylTubulin	Primary mouse antibody	P7

Table S10. Antibodies and conjugated DNA docking strands for multiplexed super-resolution PAINT imaging.

WF_FWHM	SIM_FWHM	Ratio
358.9	178.5	2.0
346.6	179.5	1.9
303.6	188.0	1.6
301.4	149.6	2.0
392.8	186.6	2.1
449.3	224.6	2.0
251.9	139.7	1.8
348.2	194.9	1.8
363.0	169.6	2.1
333.6	149.6	2.2
404.2	175.7	2.3
316.8	177.9	1.8
436.6	205.7	2.1
382.6	171.2	2.2
510.6	226.2	2.3
426.0	222.5	1.9
305.1	155.8	2.0
360.0	200.2	1.8
299.0	157.5	1.9
332.4	139.6	2.4

Table S11. Full width at half maximum data of microtubule cross-sections obtained from SIM alphaTubulin imaging.

Binding scheme	Transient	Semi-transient	Stable
Pros	1. Fast blinking frequency that allows DNA-PAINT imaging 2. Easy removal of signal from the previous cycle 3. Resistant to photobleaching 4. Faster imaging as no need to remove excessive imager strands	1. Longer binding duration on docking sites enables confocal and other platform imaging 2. Easy removal of signal from the previous cycle 3. Resistant to photobleaching 4. Faster imaging as no need to remove excessive imager strands	1. Superior signal-to-background ratio 2. Suitable for widefield and STORM imaging
Cons	1. Only suitable for DNA-PAINT imaging 2. Requires high signal-to-background ratio microscopy (e.g. TIRF, light sheet, spinning disc confocal) for imaging	1. Not suitable for STORM imaging. Widefield imaging requires post-imaging deconvolution processing. 2. Lower signal-to-background compared with stable binding; requires experimental adjustment of imager strand concentration and laser intensity to get optimal imaging setting	1. Requires long incubation time and additional wash to remove excessive imager strands prior to imaging. 2. Requires harsher washing condition (e.g. 30% formamide for 12mer) to remove signal from the previous cycle. 3. Sensitive to photobleaching
Application	DNA-PAINT	Confocal, SIM, STED, Expansion microscopy	Widefield, Confocal, SIM, STED, STORM, Expansion microscopy

Table S12. Comparison between transient, semi-transient and stable DNA binding schemes.

Movie caption:

3D views of multi-targets in fixed mouse hippocampal neuron cultures. A movie was created using Imaris for 3D slicing views of the targets shown in Figure 2. Mouse hippocampal neurons were fixed using PFA and stained to target SynapsinI, vGAT, MAP2, pNFH, AlphaTubulin, AcetylTubulin, GFAP, and DAPI.

References

(1) Behbod, F.; Kittrell, F. S.; LaMarca, H.; Edwards, D.; Kerbawy, S.; Heestand, J. C.; Young, E.; Mukhopadhyay, P.; Yeh, H. W.; Allred, D. C.; Hu, M.; Polyak, K.; Rosen, J. M.; Medina, D. *Breast Cancer Res* **2009,** 11, (5), R66.

(2) Jungmann, R.; Avendano, M. S.; Woehrstein, J. B.; Dai, M.; Shih, W. M.; Yin, P. *Nat Methods* **2014,** 11, (3), 313-8.

(3) Guizar-Sicairos, M.; Thurman, S. T.; Fienup, J. R. *Opt Lett* **2008,** 33, (2), 156-8.

(4) Agasti, S. S.; Wang, Y.; Schueder, F.; Sukumar, A.; Jungmann, R.; Yin, P. *Chem Sci* **2017,** 8, (4), 3080-3091.

(5) Gerdes, M. J.; Sevinsky, C. J.; Sood, A.; Adak, S.; Bello, M. O.; Bordwell, A.; Can, A.; Corwin, A.; Dinn, S.; Filkins, R. J.; Hollman, D.; Kamath, V.; Kaanumalle, S.; Kenny, K.; Larsen, M.; Lazare, M.; Li, Q.; Lowes, C.; McCulloch, C. C.; McDonough, E.; Montalto, M. C.; Pang, Z.; Rittscher, J.; Santamaria-Pang, A.; Sarachan, B. D.; Seel, M. L.; Seppo, A.; Shaikh, K.; Sui, Y.; Zhang, J.; Ginty, F. *Proc Natl Acad Sci U S A* **2013,** 110, (29), 11982-7.

(6) Glass, G.; Papin, J. A.; Mandell, J. W. *J Histochem Cytochem* **2009,** 57, (10), 899-905.

(7) Lin, J. R.; Fallahi-Sichani, M.; Sorger, P. K. *Nat Commun* **2015,** 6, 8390.

(8) Pirici, D.; Mogoanta, L.; Kumar-Singh, S.; Pirici, I.; Margaritescu, C.; Simionescu, C.; Stanescu, R. *J Histochem Cytochem* **2009,** 57, (6), 567-75.

(9) Micheva, K. D.; Smith, S. J. *Neuron* **2007,** 55, (1), 25-36.

(10) Tam, J.; Cordier, G. A.; Borbely, J. S.; Sandoval Alvarez, A.; Lakadamyali, M. *PLoS One* **2014,** 9, (7), e101772.

(11) Friedenberger, M.; Bode, M.; Krusche, A.; Schubert, W. *Nat Protoc* **2007,** 2, (9), 2285-94.

(12) Schubert, W.; Bonnekoh, B.; Pommer, A. J.; Philipsen, L.; Bockelmann, R.; Malykh, Y.; Gollnick, H.; Friedenberger, M.; Bode, M.; Dress, A. W. *Nat Biotechnol* **2006,** 24, (10), 1270-8.

(13) Duose, D. Y.; Schweller, R. M.; Hittelman, W. N.; Diehl, M. R. *Bioconjug Chem* **2010,** 21, (12), 2327-31.

(14) Schweller, R. M.; Zimak, J.; Duose, D. Y.; Qutub, A. A.; Hittelman, W. N.; Diehl, M. R. *Angew Chem Int Ed Engl* **2012,** 51, (37), 9292-6.

(15) Zrazhevskiy, P.; Gao, X. *Nat Commun* **2013,** 4, 1619.

(16) Zimmermann, T.; Marrison, J.; Hogg, K.; O'Toole, P. *Methods Mol Biol* **2014,** 1075, 129-48.

(17) Zhang, Z.; Kenny, S. J.; Hauser, M.; Li, W.; Xu, K. *Nat Methods* **2015,** 12, (10), 935-8.

(18) Giesen, C.; Wang, H. A.; Schapiro, D.; Zivanovic, N.; Jacobs, A.; Hattendorf, B.; Schuffler, P. J.; Grolimund, D.; Buhmann, J. M.; Brandt, S.; Varga, Z.; Wild, P. J.; Gunther, D.; Bodenmiller, B. *Nat Methods* **2014,** 11, (4), 417-22.

(19) Levenson, R. M.; Borowsky, A. D.; Angelo, M. *Lab Invest* **2015,** 95, (4), 397-405.

(20) Angelo, M.; Bendall, S. C.; Finck, R.; Hale, M. B.; Hitzman, C.; Borowsky, A. D.; Levenson, R. M.; Lowe, J. B.; Liu, S. D.; Zhao, S.; Natkunam, Y.; Nolan, G. P. *Nat Med* **2014,** 20, (4), 436-42.